Journal of Power Sources 195 (2010) 5889–5895

Contents lists available at ScienceDirect

Journal of Power Sources

journal homepage: www.elsevier.com/locate/jpowsour

Functionalization of electrochemically prepared titania nanotubes with Pt for application as catalyst for fuel cells

Fathy M.B. Hassan, Hiroshi Nanjo*, Shanmugam Venkatachalam, Mitsuhiro Kanakubo, Takeo Ebina

AIST, RC-CCP, 4-2-1 Nigatake, Miyagino-ku, Sendai 983-8551, Japan

ARTICLE INFO

Article history:
Received 29 September 2009
Received in revised form
11 December 2009
Accepted 11 December 2009
Available online 22 December 2009

Keywords:
Titania nanotubes
Anodization
Electrochemical catalyst
Fuel cells
Methanol oxidation

ABSTRACT

Titania nanotubes (TiNTs) were prepared by electrochemical anodization and were used as a support for depositing Pt. After annealing the TiNTs changed to crystalline anatase phase and were doped with carbon. The TiNTs/Pt/C was tested as electrode for electrochemical catalysis of methanol oxidation. The composite catalyst activities were measured by cyclic voltammetry in 1 M CH_3OH + 1 M H_2SO_4. The results demonstrated that TiNTs/Pt/C can greatly enhance the catalytic activity of methanol oxidation. The CO stripping led to the increase in the current peak of methanol oxidation due to activating the catalyst surface by point defect formation. Moreover, the higher ratio of the forward anodic peak current to the reverse anodic peak current indicates more effective removal of the poisonous species.

1. Introduction

The quest for alternative energy sources is one of the most important and exciting challenges facing science and technology in the 21st century. The progress in materials with nanostructure has created opportunities for progress in new energy devices. Fuel cells are attractive power sources due to their high energy density and environment friendly. Recently, there has been an increasing interest in the development of direct methanol fuel cells (DMFCs). DMFCs are considered to be promising power sources for portable applications due to its high energy density, ease of handling liquid fuel, low operating temperatures and quick start up [1–4]. However, the major problems of electrocatalyst in DMFC are the high loading of Pt and deactivation of Pt electrocatalyst [4–7]. It has been proved that the support materials in electrocatalysts play an important role to the electrochemical performance [8]. Though improvement has been made in the catalytic activity and stability of the electrocatalyst by effectively dispersing Pt particles onto the various electronically conducting supports, much effort is still continuing to improve the performance of fuel cells.

Titania nanotubes, TiNTs, is a wide bandgap semiconducting material, hence it has many important applications to photocatalysts, gas sensors, and photovoltaic cells. The combination of its intrinsic bulk properties with the nano-tubular structures is expected to lead to achieving higher performance [9–12]. The nanotubes array allows for the precise design and control of the geometrical features, allowing one to achieve a material with specific light absorption and propagation characterization [13,14] with the aligned porosity, crystallinity, and oriented nature of the nanotubes arrays making them attractive electron percolation pathways for vectorial charge transfer between interfaces [15–17].

Ti and TiO_2 have been used as anodes and/or cathodes for electrochemical reactions of technological interests such as oxygen and chlorine evolution, the reduction of oxygen and the methanol electrochemical oxidation reactions [18–20]. It has been reported that doping the Ti/TiO_2 with noble metals like Pt can improve its electro-catalytic properties [21,22]. As a support material, TiO_2 was used in several forms e.g. solution deposited TiO_2 nanoparticles [23], thermal oxidation of Ti foil at 850 °C [20], and TiO_2 nanotubes that were prepared by hydrothermal treatment of titania nanopowder [24,25]. TiNTs that were prepared by this method have very large surface area and unidimensional nanostructure, however they are randomly laying on the electrode surface [24,25]. TiNTs prepared by electrochemical anodization [26–28] provide self-organized nanotubes that are perpendicular to the electrode surface. This is expected to provide larger surface area for larger distribution of Pt nanoparticles with smaller mass which means a lower loading of Pt and a higher electro-catalytic efficiency.

The aim of this study was to prepare TiNTs by electrochemical anodization of titanium. After that, dispersed Pt nanoparticles were sputter deposited on the TiNTs. After annealing the electro-catalytic

* Corresponding author. Tel.: +81 70 6953 8414; fax: +81 22 237 7027.
E-mail address: hi-nanjo@aist.go.jp (H. Nanjo).

0378-7753/$ – see front matter © 2009 Elsevier B.V. All rights reserved.
doi:10.1016/j.jpowsour.2009.12.053

efficiency of this electrode was studied for the electrochemical oxidation of methanol in sulfuric acid.

2. Experimental

In the electrochemical anodization process the working electrode was pure titanium (99.5% and thickness 0.5 mm) was purchased from Nilaco, Japan. Pieces of 1.5 cm × 1.5 cm were used in all experiments. Before anodization, the samples were sonicated consecutively with acetone, 2-propanol and methanol, then rinsed with deionized (DI) water and dried in air stream. Electrochemical anodization was conducted using Gamry PTC1 test cell. Two electrolytes were used, ethylene glycol (EG) + 2 vol% H_2O + 0.3 wt% NH_4F and glycerol (Gly) + 14 vol%H_2O + 0.14 M NH_4F. All chemicals were purchased from Wako, Japan. The anodization was conducted using a two-electrode cell with the titanium plate as working electrode and platinum coil as the counter electrode. It is important to note that the cell used for anodization was two electrodes cell and did not feature a third reference electrode. The measured voltages were referenced to a platinum quasi-reference potential. As a result of this the measurements reflect the response not just of the working electrode but of the entire cell. The electrochemical device used was a potentiostat/galvanostat HA-3001A equipped with arbitrary function generator HB-105, both were purchased from Hokuto-Denko Corp., Japan. The potential was swept from 0 V to 30 V or 40 V at a rate of 200 mV s^{-1} followed by holding for 4 h.

Pt nanoparticles were sputtered and deposited on the as-anodized samples by using magnetron ion sputter, Vacuum Device Inc., Japan. The deposition conducted at room temperature in air at ~2×10^{-2} Pa for 4 min. After the deposition the samples were annealed at 450 °C for 1 h.

The efficiency of the electrode as electrocatalyst was determined by using cyclic voltammetry. Solartron SI1287 (potentiostat/galvanostat) equipped with an USB electrochemical interface and driven GEPS software was used for electrochemical experiments. A conventional three-electrode cell was used at room temperature (ca. 25 °C). A silver/silver chloride electrode (Ag/AgCl, saturated KCl) and a platinum coil were used as the reference and counter electrodes, respectively. The electrolyte was 1 M H_2SO_4 + 1 M CH_3OH. These chemicals were purchased from Wako, Japan and was prepared using deionized water. The pHs of 1 M H_2SO_4 and 1 M H_2SO_4 + 1 M CH_3OH solutions measured at 25 °C were −0.30 and −0.29, respectively. In this paper all potentials are referenced to reversible hydrogen electrode, RHE, unless otherwise stated. The electrode prepared based on anodization in ethylene glycol (EG) + 2 vol% H_2O + 0.3 wt% NH_4F is denoted as EG-TiNT/Pt/C and the electrode prepared based on anodization in Glycerol (Gly) + 14 vol%H_2O + 0.14 M NH_4F is denoted as Gly-TiNT/Pt/C.

The morphology of the nanostructure was inspected by a field emission scanning electron microscope, FESEM (S-4800, Hitachi). Another SEM (JSM-5600LV, JEOL) was used for EDX analysis. The annealed anodized surface structure was analyzed by X-ray diffractometer (XRD, RINT 2200VK/PC, Rigaku) operating at 40 kV and 30 mA. The source of the X-ray radiation was Cu Kα, and the scan rate was set to 2° min^{-1}.

3. Results and discussion

3.1. Preparation of TiNTs

In order to prepare self-organized TiNTs we anodized Ti samples in two solutions. Fig. 1 shows the variation of current with time during anodization of Ti in EG–2 vol% H_2O–0.3 wt% NH_4F at 60 V and in Gly–14vol%H_2O–0.14 M NH_4F at 30 V for 5 h. The anodization started by building a barrier base layer where the potential was scanned with a ramping rate of 200 mV s^{-1} from 0 to the corresponding hold potential of 30 V and 60 V. During holding the potential the current decreases to an equilibrium state and the TiNTs are developed. TiO_2 base layer continues to develop by oxidation of titanium at high potential according to the following equation:

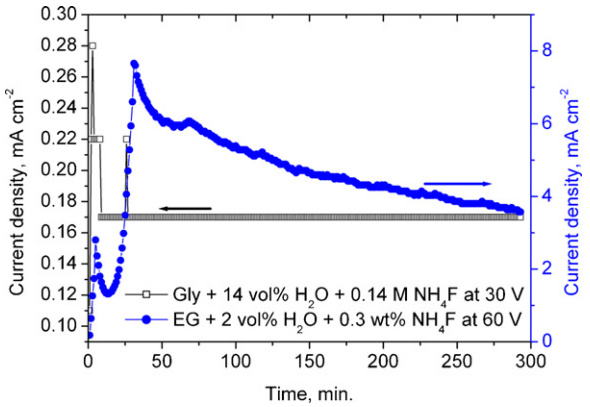

Fig. 1. Current–time relations during the anodization of Ti for 5 h in (●) EG–2 vol% H_2O–0.3 wt% NH_4F at 60 V and (□) Gly–14vol%H_2O–0.14 M NH_4F at 30 V.

$$Ti_{(s)} + 2H_2O_{(l)} = TiO_{2(s)} + 4H^+ + 4e^- \quad (1)$$

Eventually, TiO_2 is dissolved by fluoride (Field assisted dissolution) generating pores:

$$TiO_2 + 4H^+ + 6F^- \rightarrow [TiF_6]_{(aq)}^{2-} + 2H_2O \quad (2)$$

The viscosity and composition of the electrolyte play important roles in determining both the shape of the current–time curves and the morphology of the nanotubes. The glycerol-based electrolyte has higher viscosity and lower potential which lead to difficult diffusion and slower reaction 1 and 2 and consequently a lower current. The steady state current is almost constant, which is reflecting stability of the electrolyte. The ethylene glycol based electrolyte with less viscosity and high potential show higher anodization current, which decreases with time of anodization. This reflects higher rate of reactions 1 and 2 and higher growth rate of TiNTs.

3.2. Morphology and composition of the platinized TiNTs

Fig. 2 shows FESEM images of the surface of the electrode during several stages of the preparation. Fig. 2A shows the as-anodized TiNTs on the titanium sample in the EG-based electrolyte. The image shows clearly the self-organized nature of the TiNTs obtained by this anodization process. The cross section, image B, indicates that the length of the nanotubes is ca. 15 μm whereas image A shows that the average diameters are in the range of 90–100 nm. Platinum nanoparticles are deposited by physical vapor deposition method using magnetron sputtering at room temperature. The coating elapsed for 4 min and led to that the Pt particles are deposited on the mouths of the TiNTs. They did not block the tubes and allowed some holes in the order of ~20–30 nm. Fig. 2C shows the surface after Pt sputtering. The samples were weighed before and after Pt deposition, by using sensitive microbalance, to estimate the Pt loading. The Pt was loaded about 55 μg cm^{-2}. The as-prepared TiNTs are amorphous. The platinized TiNTs were annealed at 450 °C in air for 1 h in order to render them crystalline. Fig. 2D shows the morphology of the surface after annealing. The annealing process did homogenize and crystallize the surface as well. Whereas the as-anodized TiNTs appear to stick to each other with negligible intertubular distances, the annealed

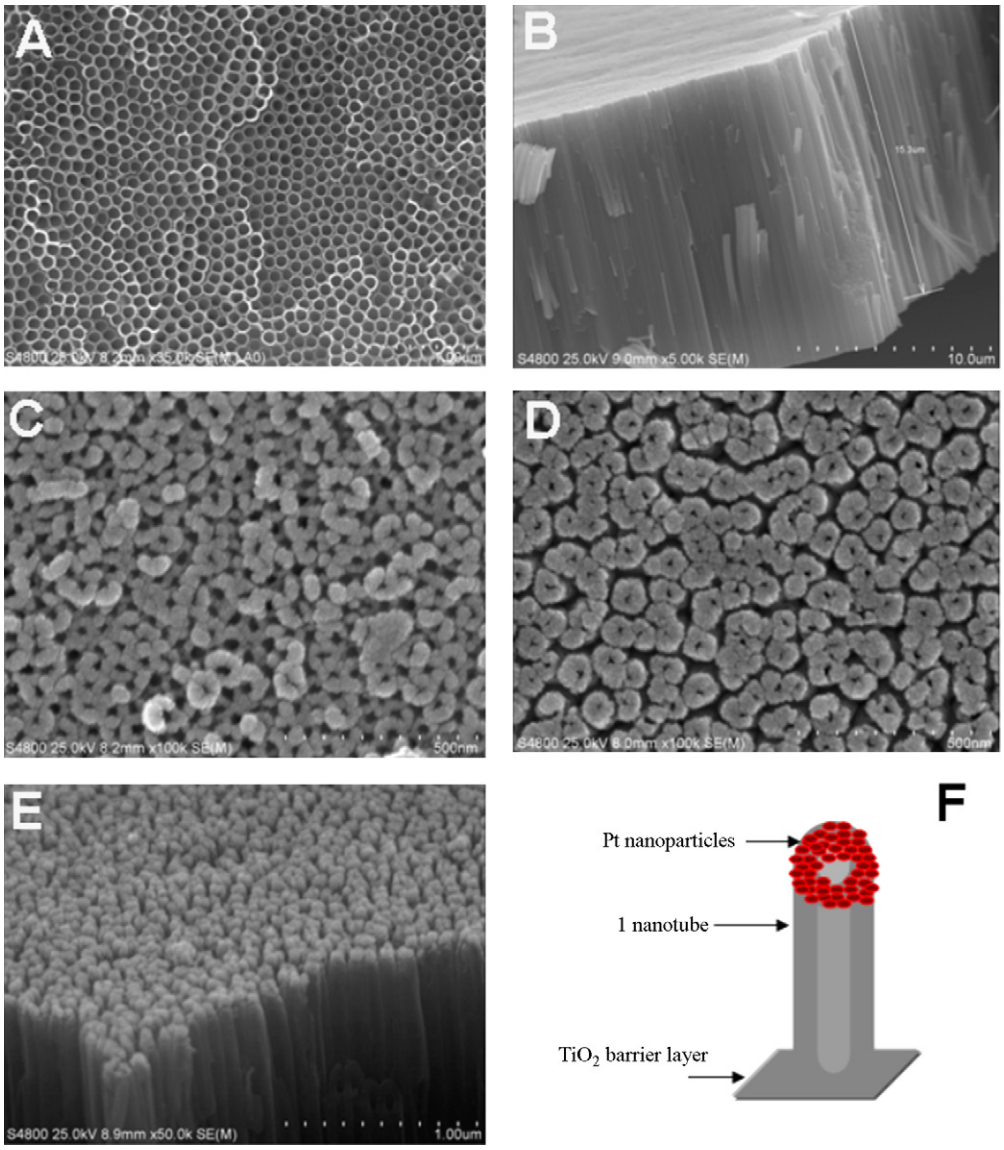

Fig. 2. FESEM images of the EG-TiNT/Pt/C electrode surface showing different treatment stages: (A) as-anodized, (B) cross section of the as-anodized, (C) after depositing Pt on the as-anodized sample (A), (D) after annealing C at 450 °C for 1 h, (E) side view of (D), and (F) a schematic of 1 TiNT with Pt nanoparticles.

samples showed some little increase in the intertubular distances, see Fig. 2D. In addition, Pt nanoparticles are redistributed and are arranged on the mouths of the nanotubes. This is attributed to the relaxation of the TiNTs/Pt after exposure to the annealing temperature. The nanotubes are held on the Ti base through a TiO_2 base layer [28] and the Pt nanoparticles are decorating their mouths, as shown schematically in Fig. 2F. A lateral view from the side for the TiNTs with the top functionalized by Pt is shown in Fig. 2E.

Fig. 3 shows FESEM images of the sample anodized in glycerol-based electrolyte. Image A shows that homogeneously self-organized TiNTs are covering the surface of the as-anodized sample. The figure shows that in case of the anodization in Gly-based electrolyte there are wider intertubular distances as compared with anodization in EG-based electrolyte. The cross section, Fig. 3B, estimates the average height of the TiNTs of ca. 7 μm. The difference in height with EG-based electrolyte indicates that the growth rate of TiNTs in EG-based electrolytes is greater than that in Gly-based electrolyte. Pt nanoparticles were deposited by using the same method as mentioned previously. Image C shows the morphology after the deposition. The Pt nanoparticles covers the mouths of the nanotubes but blocking less area of the mouths compared with the previous case (EG-based electrolyte). It is believed that the presence of wider area around the nanotubes (long intertubular distances) allowed some of the Pt nanoparticles to spread widely rather than accumulate inside the mouths of the tubes. After annealing there is no dramatic change in morphology, however a slight redistribution in Pt nanoparticles was seen in image D. Image F, which shows a high magnification and a focus on a nanotube, shows the smooth distribution of the Pt nanoparticles decorating the mouth of a nanotube. In addition, they have more fine porous structure among the nanoparticles and some of the nanoparticles are distributed outside of the nanotubes.

Fig. 4 shows the XRD pattern of the annealed platinized TiNTs sample of the Gly-TiNTs/Pt/C electrode surface. XRD pattern for the as-anodized sample was placed as a reference. The XRD patterns reveal that the TiNTs have changed from amorphous to crystalline TiO_2 phases. Under the heat treatment conditions of 450 °C for 1 h in air it was possible to produce the anatase phase of the TiO_2. In addition, some peaks corresponding to Pt(0) were evidenced. The presence of sharp peaks for Ti(0) is attributed to the titanium substrate. The small peak to the left at a Bragg's angle (2θ) of about 20º is believed to be due to carbon or carbon bearing compounds.

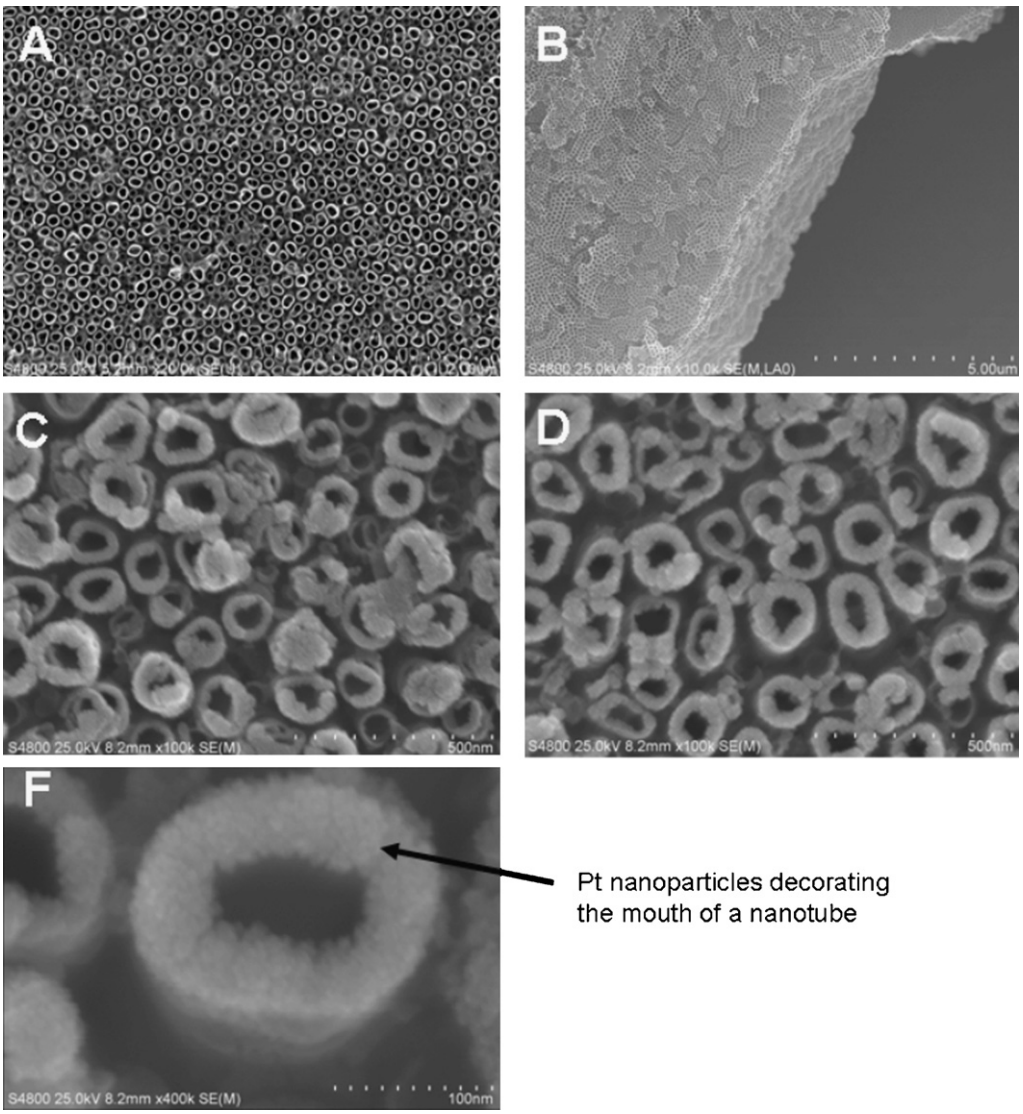

Fig. 3. FESEM images of the Gly-TiNT/Pt/C electrode surface showing different treatment stages: (A) as-anodized, (B) cross section of the as-anodized, (C) after depositing Pt on the as-anodized sample (A), (D) after annealing C at 450 °C for 1 h, and (F) higher magnification with a focus on a one-platinized annealed TiNT.

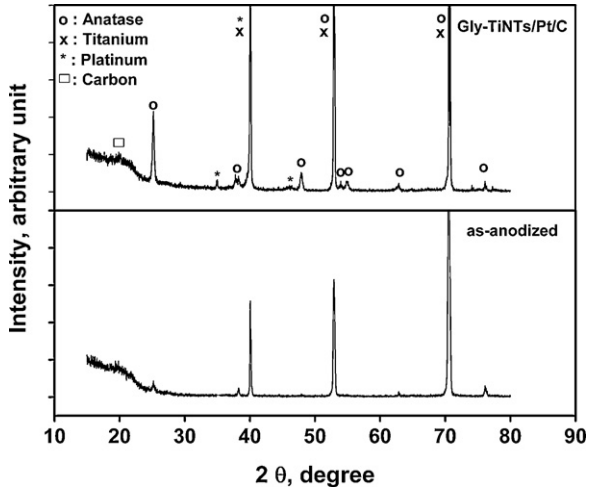

Fig. 4. XRD pattern of the annealed platinized TiNT sample of Gly-TiNT/Pt/C electrode surface and the as-anodized sample.

A similar finding for carbon doping of the TiNT after anodization in organic electrolytes was shown by Richter et al. [29].

Fig. 5 shows the EDX (energy dispersive X-ray) analysis of the Gly-TiNT/Pt/C electrode surface after annealing. The result confirms the presence of Pt in addition to Ti and O (oxygen). It is interesting to observe the presence of a peak correspond to carbon. It is not unexpected the presence of carbon since anodization in organic electrolytes leads to adsorption of organic molecules on the TiNTs. After annealing the organic molecules possibly decompose thermally leading to internal diffusion of carbon into the anatase lattice and doping the TiNT with carbon ($TiO_{2-x}C_x$). This process of carbon doping was found to increase the catalytic activity of TiO_2 [30–32]. This method provides direct short way method unlike the flame pyrolysis [30] or chemical vapor deposition [31,32] which may change the morphology of surface nanostructure.

3.3. Electrochemical performance of TiNT/Pt/C

In order to stabilize the catalyst materials before methanol oxidation experiments, cyclic voltammograms (CVs) were repeated for Gly-TiNT/Pt/C electrode in 1 M H_2SO_4 for 100 cycles at a scan rate of 50 mV s^{-1}. Fig. 6 shows the 1, 10, 30, 50, 60, 80 and 100th cycle

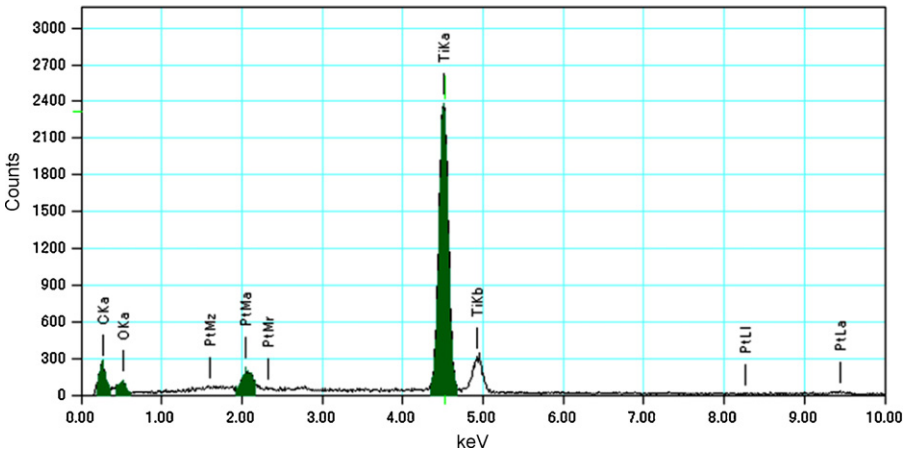

Fig. 5. EDX analysis of Gly-TiNT/Pt/C electrode surface of the annealed platinized TiNT sample.

scan of the CVs for the Gly-TiNT/Pt/C electrode in 1 M CH_3OH + 1 M H_2SO_4. Fig. 6A shows the full CV curves whereas Fig. 6B shows a focus on the peaks correspond to methanol oxidation. On the first scan to positive potentials from −0.25 V, the onset of the methanol oxidation peak was observed at about +0.2 V and a large methanol oxidation peak was observed at +0.75 on the positive irreversible scan and another acute peak of methanol oxidation was seen at +0.53 V on the reverse scan. On repeating the scan up to 100 cycles the peaks heights (oxidation current) are reduced to almost close values beyond the 10th cycle with a slight shift in the forward peak potential to noble potentials. It is noteworthy to observe that the percentage of reduction in the peak heights (i.e. in the peak current) is only about 35% of the first peak current. This means that the Gly-TiNT/Pt/C electrode is functioning as an electroactive catalyst with efficiency which is only reduce to about 65%, as estimated up to the 100th scan cycle.

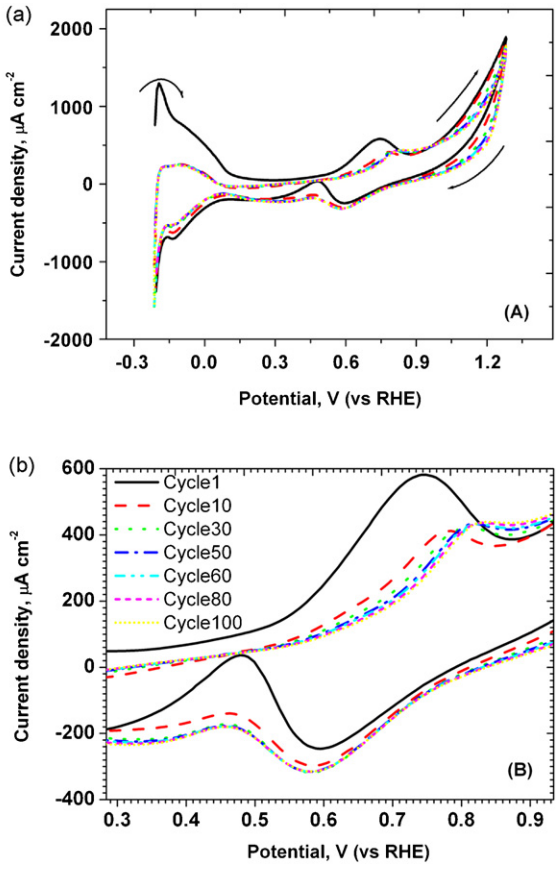

Fig. 6. (A) The 1, 10, 30, 50, 60, 80 and 100th cycle scan of the CVs for the Gly-TiNT/Pt/C electrode in 1 M CH_3OH + 1 M H_2SO_4 at a scan rate of 50 mV s^{-1}. (B) Magnification of Fig. 7A with focus on the peaks correspond to methanol oxidation.

Methanol is the lightest alcohol, so its oxidation reactions proceed relatively smooth with few intermediate reactions (or species). A well-known mechanism of methanol oxidation involves the following steps that result in the formation of some intermediates including strongly adsorbed CO species [33–39]:

$$(CH_3OH)_{soln.} \Leftrightarrow Pt\text{-}(CH_3OH)_{ads} \quad (3)$$

$$Pt\text{-}(CH_3OH)_{ads} \Leftrightarrow Pt\text{-}(CH_3O)_{ads} + H^+ + e^- \quad (4)$$

$$Pt\text{-}(CH_3O)_{ads} \Leftrightarrow Pt\text{-}(CH_2O)_{ads} + H^+ + e^- \quad (5)$$

$$Pt\text{-}(CH_2O)_{ads} \Leftrightarrow Pt\text{-}(CHO)_{ads} + H^+ + e^- \quad (6)$$

$$Pt\text{-}(CHO)_{ads} \Leftrightarrow Pt\text{-}(CO)_{ads} + H^+ + e^- \quad (7)$$

The complete methanol oxidation can occur and cause sharp increase in current:

$$Pt\text{-}(CO)_{ads} + H_2O \Leftrightarrow Pt + CO_2 + 2H^+ + 2e^- \quad (8)$$

At potentials above 0.70 V the oxidation of Pt and the formation of platinum oxides (or chemisorbed oxygen) cause a decrease in the amount of active sites available on the electrode surface, which subsequently result in a decrease in the peak current, as seen in Fig. 6A. During the backward scan, the reduction of platinum oxides to Pt(0) and the regeneration of active sites take place, therefore the further oxidation of methanol and/or methanol residues occurs on clean Pt surface and the backward peak appears at about 0.48 V. Oxidation of methanol at low potential leads to adsorption of CO species which leads to poisoning the catalyst. The surface reaction between this adsorbed CO species and the adsorbed OH species, from H_2O dissociation, leads to the formation of CO_2 and the reactivation of the catalyst.

In order to study the effect of removal of the adsorbed CO on the electrode further use, stripping voltammetry was conducted as follows: a set of 20 cycle of CVs was done for the above electrode (Gly-TiNT/Pt/C) in 1 M H_2SO_4 at a scan rate of 20 mV s^{-1} (from −0.3 to 1.0 V). During these cycles the adsorbed CO is oxidized. Fig. 7 shows CVs before and after stripping of the adsorbed CO of the Gly-TiNT/Pt/C electrode in 1 M CH_3OH + 1 M H_2SO_4. It seems, as may be expected, that desorption of CO has activated the electrode surface for oxidation of methanol once again. To see whether this treatment has a long effect on the efficiency and electrode stability we have done chronoamperometric curve by holding at the potential of

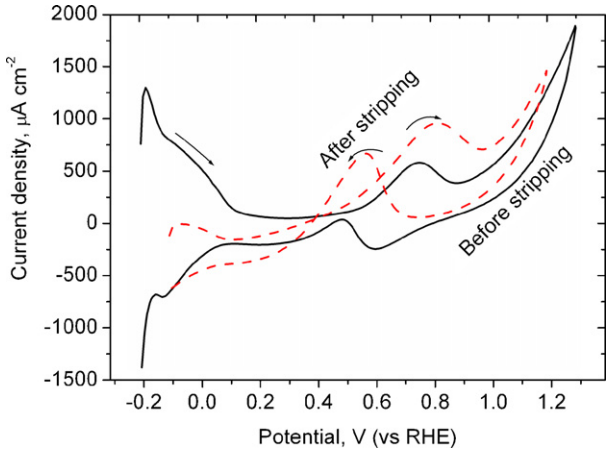

Fig. 7. Cyclic voltammograms before and after stripping of the adsorbed CO of Gly-TiNT/Pt/C electrode in 1 M CH_3OH + 1 M H_2SO_4 at a scan rate of 50 mV s^{-1}.

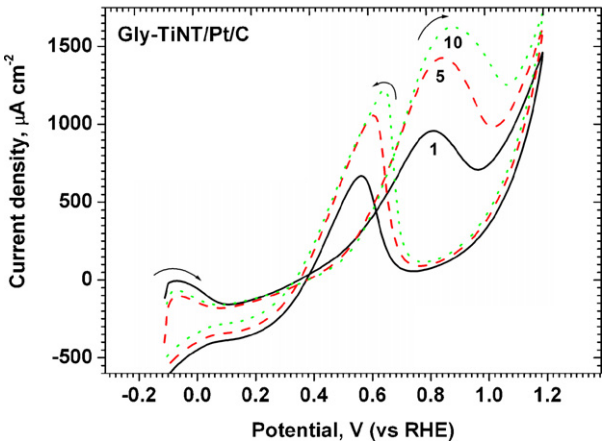

Fig. 9. Cyclic voltammograms after stripping treatment of Gly-TiNT/Pt/C electrode in 1 M CH_3OH + 1 M H_2SO_4 at a scan rate of 50 mV s^{-1}.

methanol oxidation (+0.75 V) for 1 h and monitoring the resulting current as a function of time. The results are plotted in Fig. 8 which compare before and after CO stripping. From these curves it can be inferred that the treatment of the poisoned surface by stripping the CO has prolonged the activation of the electrode i.e. the consecutive oxidation of methanol do not re-adsorb as much CO as has done initially or the surface has become more active to enhance the oxidation of CO_{ads} with the OH_{ads} to form CO_2. The peak current corresponding to methanol oxidation is higher for the after stripping than that before stripping for almost 1 h of potentiostatic holding. Moreover, a new set of CVs scans after the stripping treatment was recorded for Gly-TiNT/Pt/C electrode in 1 M CH_3OH + 1 M H_2SO_4 at a scan rate of 50 mV s^{-1}. The results indicate a considerable increase in the heights (peak current) of the forward and backward peaks correspond to methanol oxidation. In addition, the potential of the anodic peak on the anodic sweep is shifted to more positive potentials. This result was plotted in Fig. 9 which shows the cycle's no. 1, 5 and 10 of the CVs.

The stripping treatment of the electrode at potentials higher than the effective potential of CO_{ads} oxidative desorption leads to surface free of poison and to activate the catalyst surface by point defect formation and surface oxidation [20]. The activity of the surface prepared in this way depends on the number of point defects introduced during anodic scan or potentiostatic holding, which increases with potential [40–42]. The ratio of the forward anodic peak current (I_f) to the reverse anodic peak current (I_b) can be used to describe the catalyst tolerance to accumulation of carbonaceous species [43–47]. A higher ratio indicates more effective removal of the poisoning species on the catalyst surface. The I_f/I_b ratio of Gly-TiNT/Pt/C, as estimated from Fig. 10 is about 1.2, which indicates high catalyst tolerance.

Fig. 10 is a set of CVs conducted on the electrode EG-TiNT/Pt/C which was anodized in EG-based electrolyte and was subjected to the same sequence of treatment as Gly-TiNT/Pt/C. It is almost very similar to the results of Gly-TiNT/Pt/C (Fig. 9), however the values of I_f and I_b are slightly lower. This can be explained in terms of the morphology and Pt distribution on both electrodes. In case of EG-TiNT/Pt/C the TiNT are closer to each other and the Pt nanoparticles covered (and blocked) greater area on the mouths of the tubes, so it is expected that the overall surface area of Pt distribution is less. In case of Gly-TiNT/Pt/C there is a wider surface area among the nanotubes. Consequently, during Pt sputtering, the nanoparticles are distributed on the mouths and on some of the outer sides of the TiNTs, hence covering a wider surface area which lead to more active sites and hence the observed higher current.

Figs. 9 and 10 show that the CH_3OH oxidation peaks heights increase by increasing the number of scans. The result is supported by the work of Hepel et al. [20] who found that, in case of TiO_2/PtRu, depoisoning leads to a large current loop extending the methanol anodic oxidation currents. This observation, as

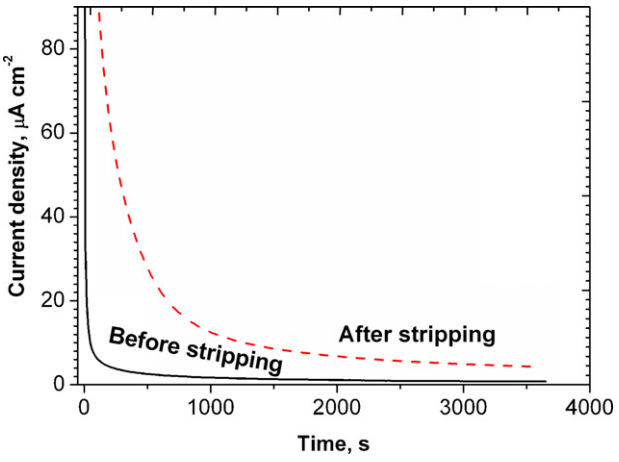

Fig. 8. Variation of current with time during potentiostatic holding at +0.75 V before and after stripping of the adsorbed CO of Gly-TiNT/Pt/C electrode in 1 M CH_3OH + 1 M H_2SO_4.

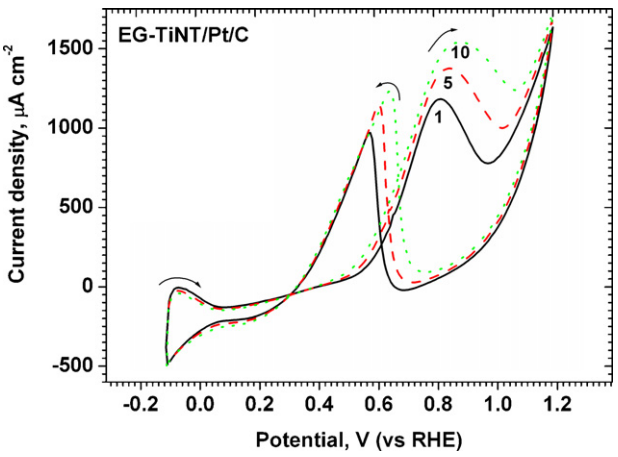

Fig. 10. Cyclic voltammograms after stripping treatment of EG-TiNT/Pt/C electrode in 1 M CH_3OH + 1 M H_2SO_4 at a scan rate of 50 mV s^{-1}.

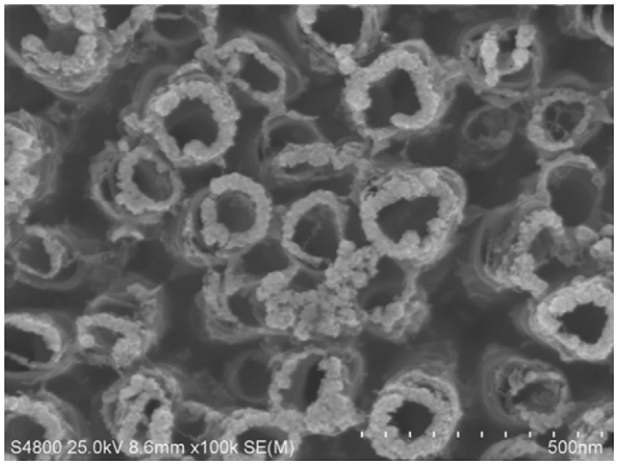

Fig. 11. An FESEM image of the Gly-TiNT/Pt/C electrode after 350 cycles of CVs in 1 M CH_3OH + 1 M H_2SO_4 at a scan rate of 50 mV s^{-1}.

well as the high I_f/I_b ratio, indicates that the TiNT/Pt/C electrocatalyst has a long retention of active surface for methanol electro-oxidation.

Fig. 11 shows an FESEM image of the Gly-TiNT/Pt/C electrode after 350 cycles of CVs in 1 M CH_3OH + 1 M H_2SO_4. The Pt covered TiNTs appears to be affected. The Pt nanoparticles appear to be redistributed around the mouths of the nanotubes with some dislocation. However, the majority of Pt nanoparticles still coating the mouths of the TiNTs. The figure reveals the relative high stability of the deposited Pt layer regardless sever testing environment of over 350 CV cycles.

4. Conclusions

The results presented in this study indicated that the catalytic activities of TiNT/Pt/C catalyst for methanol electro-oxidation are enhanced due to the large surface area of a low loading of Pt on the support by TiNTs. The CO stripping led to increasing the current peak of methanol oxidation due to activating the surface by point defect formation. The support by TiNTs (anatase) led to higher ratio of forward anodic peak current to the backward anodic peak current indicating more effective removal of the poisoning species (high catalyst tolerance). The results point out that by varying the electronic, chemical, and structural properties of underlying supporting films, extremely low precious metal loading and high catalytic activity can be achieved.

Acknowledgment

This work was supported in part by Iketani Science and Technology Foundation.

References

[1] T. Maiyalagan, F. Nawaz Khan, Catal. Commun. 10 (2009) 433.
[2] M.P. Hogarth, G.A. Hards, Platinum Met. Rev. 40 (1996) 150.
[3] T.R. Ralph, Platinum Met. Rev. 41 (1997) 102.
[4] A. Hamnett, Catal. Today 38 (1997) 445.
[5] R. Dillon, S. Srinivasan, A.S. Arico, V. Antonucci, J. Power Sources 127 (2004) 112.
[6] A.S. Arico, V. Baglio, E. Modica, A. Blasi, V. Antonucci, Electrochem. Commun. 6 (2004) 164.
[7] S. Wasmus, A. Kuver, J. Electroanal. Chem. 461 (1999) 14.
[8] M. Carmo, V.A. Paganin, J.M. Rosolen, E.R. Gonzalez, J. Power Sources 142 (2005) 169.
[9] C.L. Huisman, A. Goossens, J. Schoonman, Chem. Mater. 15 (2003) 4617.
[10] T. Tachikawa, S. Tojo, M. Fujitsuka, T. Sekino, T. Majima, J. Phys. Chem. B 110 (2006) 14055.
[11] O.K. Varghese, D. Gong, M. Paulose, K.G. Ong, E.C. Dickey, C.A. Grimes, Adv. Mater. 15 (2003) 624.
[12] Y. Ohsaki, N. Masaki, T. Kitamura, Y. Wada, T. Okamoto, T. Sekino, K. Niihara, S. Yanagida, Phys. Chem. Chem. Phys. 7 (2005) 4157.
[13] K.G. Ong, O.K. Varghese, G.K. Mor, C.A. Grimes, J. Nanosci. Nanotechnol. 5 (2005) 1801.
[14] K.G. Ong, O.K. Varghese, G.K. Mor, K. Shankar, C.A. Grimes, Sol. Energy Mater. Sol. Cells 91 (2007) 250.
[15] G.K. Mor, K. Shankar, M. Paulose, O.K. Varghese, C.A. Grimes, Nano Lett. 6 (2006) 215.
[16] K. Zhu, N.R. Neale, A. Miedaner, A.J. Frank, Nano Lett. 7 (2007) 69.
[17] A.J. Frank, N. Kopidakis, van de Lagemaat, J. Coord. Chem. Rev. 248 (2004) 1165.
[18] K. Tammeveski, T. Tenno, A. Rosental, P. Talonen, L.-S. Johansson, L. Niinisto, Electrochem. Soc. 146 (1999) 669.
[19] M.I. Rojas, M.J. Esplandiu, L.B. Avalle, E.P.M. Leiva, V.A. Macagno, Electrochim. Acta 43 (1998) 1785.
[20] M. Hepel, I. Kumarihamy, C.J. Zhong, Electrochem. Commun. 8 (2006) 1439.
[21] K. Tammeveski, M. Arulepp, T. Tenno, C. Ferrater, J. Claret, Electrochim. Acta 42 (1997) 2961.
[22] M.F. Weber, M.J. Dignam, S.M. Park, R.D. Venter, Electrochem. Soc. 133 (1986) 734.
[23] H.-j. Kim, D.-y. Kim, H. Han, Y.-g. Shul, J. Power Sources 159 (2006) 484.
[24] M. Wang, D.-j. Guo, H.-l. Li, J. Solid State Chem. 178 (2005) 1996.
[25] H. Song, X. Qiu, X. Li, F. Li, W. Zhu, L. Chen, J. Power Sources 170 (2007) 50.
[26] F.M. Bayoumi, B.G. Ateya, Electrochem. Commun. 8 (2006) 38.
[27] F.M.B. Hassan, H. Nanjo, M. Kanakubo, I. Ishikawa, M. Nishioka, e-J. Surf. Sci. Nanotechnol. 7 (2009) 84.
[28] F.M.B. Hassan, H. Nanjo, H. Tetsuka, M. Kanakubo, T. Aizawa, M. Nishioka, T. Ebina, A. Bond, Electrochem. Soc. 156 (2009) K227.
[29] C. Richter, Z. Wu, E. Panaitescu, R.J. Willey, L. Menon, Adv. Mater. 19 (2007) 946.
[30] S.U.M. Khan, M. Al-Shahry, M. Ingler, Science 297 (2002) 2243.
[31] A. Ghicov, J.M. Macak, H. Tsuchiya, J. Kunze, V. Haeublein, L. Frey, P. Schmuki, Nano Lett. 6 (2006) 1080.
[32] J.H. Park, S. Kim, A. Bard, Nano Lett. 6 (2006) 24.
[33] M.H. Pournaghi-Azar, B. Habibi-A, J. Electroanal. Chem. 580 (2005) 23.
[34] L. Niu, Q. Li, F. Wei, S. Wu, P. Liu, X. Cao, J. Electroanal. Chem. 578 (2005) 331.
[35] F. Vigier, F. Gloaguen, J.M. Léger, C. Lamy, Electrochim. Acta 46 (2001) 4331.
[36] P. Ross, N. Markovic, Cattech 4 (2000) 110.
[37] M.H. Poumaghi-Azar, B. Habibi, J. Electroanal. Chem. 601 (2007) 53.
[38] W.S. Li, L.P. Tian, Q.M. Huang, H. Li, H.Y. Chen, X.P. Lian, J. Power Sources 104 (2002) 281.
[39] R. Manohara, J.B. Goodenough, J. Mater. Chem. 2 (1992) 875.
[40] K.A. Friedrich, K.P. Geyzers, U. Linke, U. Stimming, J. Stumper, J. Electroanal. Chem. 402 (1996) 123.
[41] A.V. Petukhov, W. Akemann, K.A. Friedrich, U. Stimming, Surf. Sci. 402–404 (1998) 182.
[42] K. Itaya, S. Sugawara, K. Sashikata, N. Furuya, J. Vac. Sci. Technol. A 8 (1989) 515.
[43] Z. Liu, J.Y. Lee, W. Chen, M. Han, L.M. Gan, Langmuir 20 (2004) 181.
[44] Y. Mu, H. Liang, J. Hu, L. Jiang, L. Wan, J. Phys. Chem. B 109 (2005) 22212.
[45] R. Manoharan, J.B. Goodenough, J. Mater. Chem. 2 (1992) 875.
[46] Z. Liu, X.Y. Ling, X. Su, J.Y. Lee, J. Phys. Chem. B 108 (2004) 8234.
[47] T.C. Deivaraj, J.Y. Lee, J. Power Sources 142 (2005) 43.